Lo, Mu-Chieh; Zarzuelo, Alberto; Guzmán, Robinson; Carpintero, Guillermo. (2018). Monolithically Integrated Microwave Frequency Synthesizer on InP Generic Foundry Platform. *Journal of Lightwave Technology*, 36(19), pp. 4626 – 4632.

DOI: 10.1109/JLT.2018.2836298

Monolithically integrated microwave frequency synthesizer on InP generic foundry platform

Mu-Chieh Lo, Alberto Zarzuelo, Robinson Guzmán, and Guillermo Carpintero

(Invited Paper)

***Abstract*—A photonic integrated circuit for microwave generation is proposed and experimentally validated. On the microchip, two tunable monochromatic lasers spectrally separated by 0 - 10.7 nm are monolithically integrated with one high-speed photodiode in heterodyne configuration for enabling continuous RF synthesis from 2 to 42 GHz. Under free-running operation, the two lasers with 20 - 40 MHz optical linewidth produce RF beat note with ∼90 MHz electrical linewidth at the on-chip photodiode. This is the first demonstration of such a fully integrated microwave photonic generator developed within an open-access generic foundry platform.**

***Index Terms*—Microwave photonics, Millimeter wave, Photonic integrated circuits, Indium phosphide, Laser tuning, P-i-n diodes.**

I. Introduction

MICROWAVE photonics (MWP) brings together the best of both the optical and the electrical worlds. Over the past three 30 years, it has advanced from transmission of microwave signals through optical fiber to generation, manipulation, detection and distribution of radio-frequency (RF) signals utilizing photonic concepts and techniques [1][2]. MWP creates new opportunities for rapidly growing broadband wireless communications, which require carrier wave signals in millimeter wave (mmW) and terahertz (THz) ranges for the fifth generation (5G) systems [3][4]. A target data rate of 100 Gb/s is foreseen for wireless communications in next decade, and the trend has indicated that the carrier frequencies for broadband wireless communications are supposed to move into those mmW range and even above, as the data rate basically depends on the carrier frequency in the case of simple modulation schemes for low latency [5]. Photonics-assisted techniques reveal advantages for the generation of these carrier wave frequencies, such as low phase noise, wide frequency tuning range, and broad modulation bandwidth that are not directly reachable in the RF domain [6][7].

To date, most of the reported photonics-assisted mmW/THz sources are primarily composed of commercial off-the-shelf components owing to the availability of mature telecom-based high-frequency components, i.e. tunable single-wavelength lasers, broadband modulators and high-speed photo-detectors (PDs). However, these discrete components occupy vast space and energy, and meanwhile fiber interconnections in between deteriorate the system performance. These challenges in terms of size, weight and power (SWaP) can be addressed by photonic integration. Also, with photonic integration, a considerable reduction in alignment sensitivity, coupling losses, as well as packaging cost is achieved [8].

The authors are with the Departamento de Tecnología Electrónica, Universidad Carlos III de Madrid, Av de la Universidad, 30. 28911 Leganés, Madrid, Spain. e-mail: mlo@ing.uc3m.es

Manuscript received April 19, 2005; revised August 26, 2015.

(a) mode-locked laser for microwave pulse generation

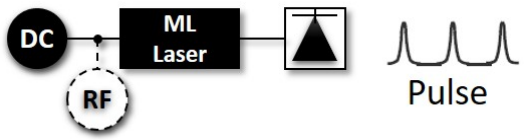

(b) optical heterodyne for continuous wave generation

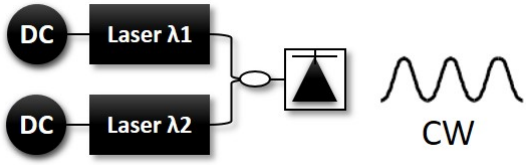

Fig. 1: (a) ML laser with PD generates pulse. It can be synchronized to an additional RF source for greater stability. (b) Optical heterodyning based on two single-wavelength lasers generates continuous wave. The generated frequency is equal to the frequency spacing between the two wavelengths.

By leveraging photonic integration, there are mainly two methods to produce optical seeds for mmW/THz generation, namely pulsed and continuous-wave (CW). Mode locking (ML) and optical heterodyning have been regarded as efficient approaches for pulse and CW formation as shown in Fig. 1(a) and Fig. 1(b), respectively [9]. Each has its own advantages and disadvantages. In ML, the spectral purity is ensured thanks to the intrinsic coherence, but the frequency is barely tunable limited by the resonator geometry [10]. In contrast, free-running optical heterodyning features a THz-scale tuning range yet an additional stabilization scheme is usually required. Such integrated tunable optical heterodyning sources based on two parallel single-mode semiconductor lasers have been demonstrated in diverse technologies [11][12][13][14][15].

In Ref. [11], two distributed feedback (DFB) lasers incorporating two multimode interference (MMI) couplers for bidirectional two-tone emission was presented to implement coherent CW THz transmitter (Tx) and receiver (Rx), however, demanding external PIN-photodiode (PD) and photoconductor for optic/electric (O/E) conversion. In Ref. [16] and [13], four-DFB arrays were deployed to extend the tuning range to above 2 THz, but incapable of on-chip O/E conversion, ei-

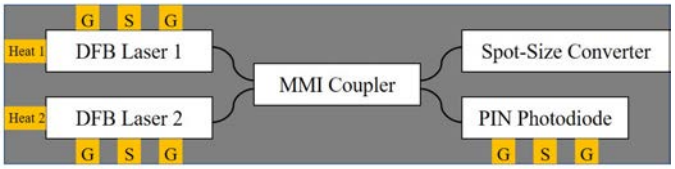

Fig. 2: The proposed optical heterodyning device structure emits both the optical signal from the spot-size converter and the electrical signal from the PIN photodiode.

ther. Currently, chip-to-chip integration approaches have been demonstrated by Ref. [14] and [15], based on III-V/polymer hybrid integration and III-V/silicon heterogeneous integration, respectively. The first fully monolithically integrated millimeter wave transmitter was demonstrated in Ref. [12] comprising two DFB lasers, combined on a multimode interference (MMI) coupler prior to uni-traveling-carrier (UTC)-PDs, developed through a dedicated fabrication process flow at III-V lab, a private R&D organization.

Open-access generic photonic integration technology potentially provides a scalable solution to the aforementioned problems which enables building a large number of both active and passive optoelectronic components on a single substrate, without the need of additional high-precision assembly. A broad variety of functionalities are thus feasible by using the standard on-chip building blocks (BBs) including, but not limited to lasers, semiconductor optical amplifiers (SOAs), phase modulators, photo-detectors (PDs), filters, multiplexers, multimode interference (MMI) couplers as well as reflectors. BBs are predefined to ease the design flow, but can also be parameterized according to process design kit (PDK) provided by foundry. The photonic integrated circuits (PICs) are manufactured within multi-project wafer (MPW) service whereby mask and wafer area are shared, and so is fabrication cost among multiple different users [17].

To the best of our knowledge, we report for the first time a fully monolithically integrated dual-wavelength optical heterodyne PIC chip, fabricated using the generic InP foundry platform at HHI [18]. The chip includes two wavelength-tunable DFB lasers, a MMI coupler and a PIN-PD for on-chip O/E conversion as shown in Fig. 2. The DFB and PIN building blocks come with Ground-Signal-Ground (GSG) coplanar waveguide supporting RF operation. An optical output of the heterodyne signal is also provided through a spot-size converter (SSC) port.

II. Device description

Fig. 3(a) illustrates the schematic layout and Fig. 3(b) presents the microscope photograph of the PIC under test. In Fig. 3(a), two DFB lasers are combining through the MMI coupler prior to the SSC as optical output, and PIN-PD as electrical output. The emission wavelengths of DFB gratings were set to have a spacing of 4 nm. Each DFB laser contains a GSG coplanar waveguide (CPW) supporting direct RF modulation, along with an internal heater for thermo-optic wavelength tuning. The gain current is injected onto the

(a) Schematic layout

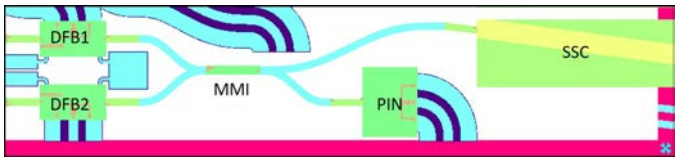

(b) Microscope photograph

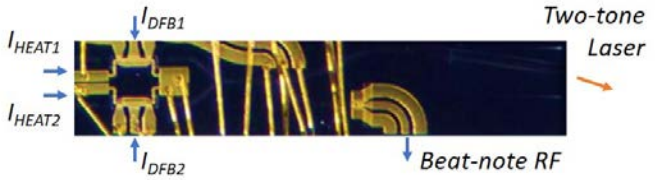

Fig. 3: (a) Schematic layout (b) Microscope photograph of the PIC under test. DFB: DFB laser. MMI: MMI coupler. SSC: Spot-size converter. PIN: PIN diode.

GSG CPW, and the bias current for heater is fed onto the heater DC pad. With the butt-joint active-passive transitions and deeply etched passive waveguide S-bends based on sine curves, allowing for continuous curvature throughout the bend [19], the ridge-waveguide stripe DFB lasers are coupled to the deeply etched 2x2 MMI coupler. Through another transition and sine bend, one of the split 3-dB MMI output is coupled to the PIN-PD for on-chip photo-detection. This BB offered by the foundry includes the PD placed on top of the waveguide for O/E conversion. It is connected with the GSG CPW in a 90° curve to simplify wire-bonding and probing. The other split 3-dB MMI output is coupled to the 7° angled SSC waveguide output, deployed for coupling light out of the chip on the anti-reflection (AR) coated front facet. In SSC, the shallowly etched waveguide is adiabatically tapered to give maximum overlap and minimum distortion with respect to standard single-mode fiber. However, in this proof-of-concept article, a lensed fiber is used to collect the light coupled from the SSC, with an additional coupling loss. which is then assessed on a Yokogawa optical spectrum analyzer (OSA). The dimension of the PIC under test is 4.5 mm x 1 mm. The $250\text{-}\mu\mathrm{m}-\mathrm{thick}$ InP chip is mounted on a 0.4-mm-thick submount and placed on a copper block with active Peltier thermoelectric cooler (TEC) on the surface, and controlled at 16°C with a Thorlabs TEC controller.

III. Characterization results

The emission wavelength of a DFB laser is a function of its bias current and temperature. Based on the data collected with the OSA, Fig. 4(a) presents the peak wavelength of each DFB at varied gain current while Fig. 4(b) presents the peak wavelength at varied heater current. In Fig. 4(a), DFB1 is lasing from 1556 nm to 1660 nm under I_{DFB1} = 30 mA - 100 mA. DFB2 emission wavelength is 1552 nm under I_{DFB2} = 30 mA, and continuously shifts up to 1556 nm as I_{DFB2} approaches 100 mA. Both DFB lasers exhibit the similar linear dependency where the peak power rises as the gain current

(a) Wavelength dependency on gain current

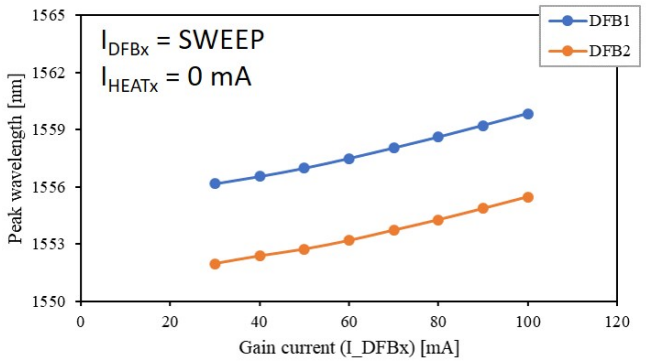

(b) Wavelength dependency on heater current

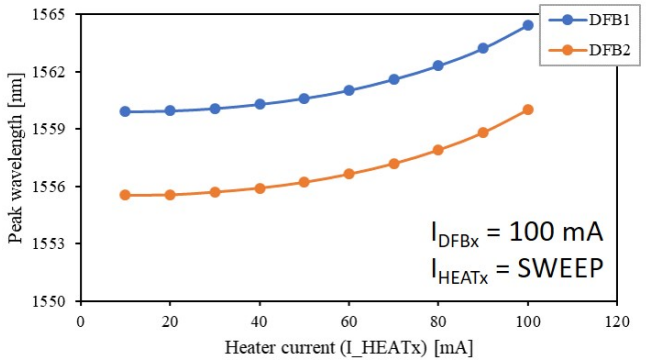

Fig. 4: (a) Schematic layout (b) Microscope photograph of the PIC under test. DFB: DFB laser. Heat: Heater pad. GND: Ground pad. MMI: MMI coupler. SSC: Spot-size converter. PIN: PIN diode.

increases, within a tuning range of 4 nm. Both DFB lasers become saturated at the bias current for gain section of 100 mA, with 0.5-mW output optical power coupled by a lensed-fiber. As shown in Fig. 4(b), the DFB1 emission wavelength is continuously and exponentially tuned under I_{DFB1} fixed at 100 mA and I_{HEAT1} varied from 10 mA to 100 mA. The DFB2 has the same dependence on heater current and the wavelength is always approximately 4 nm lower than DFB1 under the same heater current. It appears that each DFB is continuously dependent on both its gain and heater bias currents. Moreover, each DFB is affected by the bias currents of the other DFB which is discussed in next section.

Fig. 5 shows the dual wavelength emission spectra when both DFB lasers are activated simultaneously. In Fig. 5(a), a series of optical spectra are presented under the bias conditions I_{DFB1} = 90 mA, I_{DFB2} = 90 mA, I_{HEAT1} = 0 mA, and I_{HEAT2} varied from 0 mA to 90 mA in a step of 10 mA. The wavelength spacing between DFB1 and DFB2 ranges from approximately 4 nm to 1 nm as the bias current for HEAT2 I_{HEAT2} increases. During this tuning transition, the left-hand side lasing mode (DFB2) shifts exponentially upwards by >4 nm, and the right-hand side lasing mode (DFB1) does not remain unchanged. Instead, the DFB1 mode slightly shifts upwards, indicating that DFB1 is also affected by I_{HEAT2}.

(a) Two-tone spectra with spacing of 4 $\sim$ 1 nm

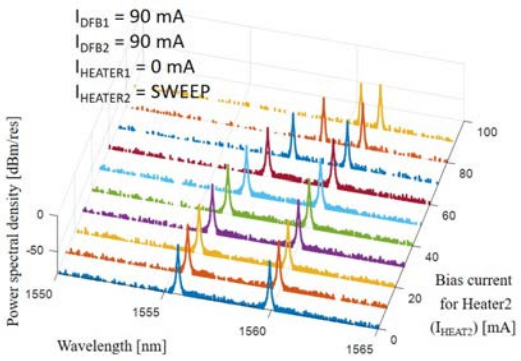

(b) Two-tone spectra with spacing of 3 $\sim$ -0.5 nm

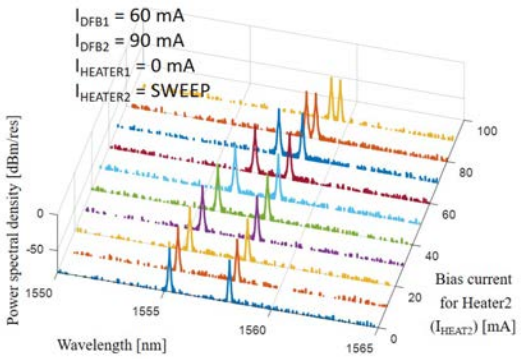

(c) Two-tone spectra with spacing of +0.5 $\sim$ -0.5 nm

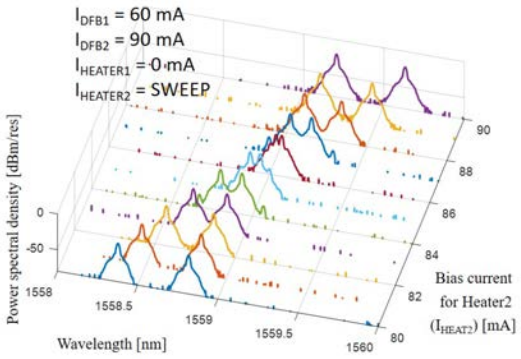

Fig. 5: Two-tone spectra (a) with I_{HEAT2} swept from 0 mA to 90 mA. (b) with I_{HEAT2} swept from 0 mA to 90 mA and a lower I_{DFB1}. (c) with I_{HEAT2} swept from 80 mA to 90 mA and a lower I_{DFB1}. The left mode (DFB2) shifts to the right as I_{HEAT2} increases. Meanwhile, the right mode (DFB1) is slightly influenced by I_{HEAT2} due to the thermal crosstalk produced at DFB2 laser diode.

It is caused by thermal crosstalk, e.g., DFB1 undergoes the accumulated heat generated by DFB2, in the presence of gain (I_{DFB2}) or heater current (I_{HEAT2}). DFB1 wavelength appears to be not only a function of I_{DFB1} and I_{HEAT1}, but also of I_{DFB2} and I_{HEAT2} which complicates the optimization of bias condition. To reduce the thermal crosstalk, the DFB1 and DFB2 components should be designed to be physically further

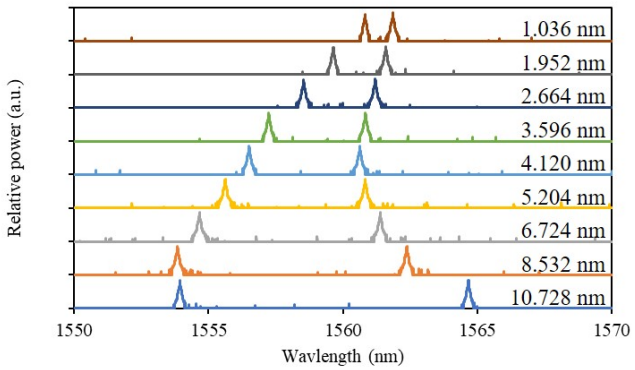

Fig. 6: Two-tone emission spectrum spaced by 1.036 ∼ 10.728 nm, corresponding to 0.13 ∼ 1.32 THz.

away from each other. Fig. 5(b) shows the two-tone emission in another scenario, I_{DFB1} = 60 mA, I_{DFB2} = 90 mA, I_{HEAT1} = 0 mA, and I_{HEAT2} varied from 0 mA to 90 mA. The initial wavelength of DFB1 is 1558 nm at I_{DFB1} = 60 mA, and also shifts slightly to the right when I_{HEAT2} rises up due to the thermal crosstalk. The wavelength spacing between DFB1 and DFB2 thus spans from 3 nm to less than 1 nm, as the bias current for HEAT2 I_{HEAT2} increases. Furthermore, the wavelength of DFB2 rises much less rapidly (<5 nm within 0 - 100 mA) than the increase in Fig. 5(a). It indicates that the tuning efficiency and precision of each laser significantly depend on the overall bias condition for both lasers, rather than on only the bias currents fed onto the laser alone. Fig. 5(c) illustrates the detail of Fig. 5(b) with a span of 2 nm and I_{HEAT2} from 80 mA to 90 mA in a step of 1 mA. Around I_{HEAT2} = 86 mA, DFB1 and DFB2 lasing modes shifts across each other where a zero-nm wavelength spacing is expected to be obtained. It is expected that under proper biasing conditions low GHz frequencies are achievable.

Fig. 6 presents the two-tone emission spectrum towards the other extreme, where the highest achievable wavelength spacing is 10.728 nm. The continuously tunable wavelength spacing is demonstrated through the series of two-tone emission spectra in C-band by carefully selecting the four bias current parameters, e.g., I_{DFB1}, I_{DFB2}, I_{HEAT1}, and I_{HEAT2}. As mentioned previously, the thermal crosstalk effect occurring in relation to unwanted ohmic heat produced by bias current, in turn weaken the tuning capability. For instance, when we are aiming for higher wavelength spacing, we should tune DFB1 up. And when DFB1 is biased with higher current, its wavelength shifts upwards and thus moves farther away from DFB2 lasing mode. Meanwhile, DFB2 receives the influence due to the heat generated in DFB1 and accordingly shifts upwards as well, but on a smaller scale, which certainly compensates the wavelength spacing increase. Therefore, the thermal crosstalk weakens the wavelength tuning capability and limits the beat-note frequency range. Despite the fact that the thermal crosstalk appears influential, a continuous tuning range up to over 10.7 nm equivalent to 1.3 THz is reached.

In Fig. 7(a), a sequence of optical spectra presenting a nonlinear effect in addition to the thermal crosstalk is shown,

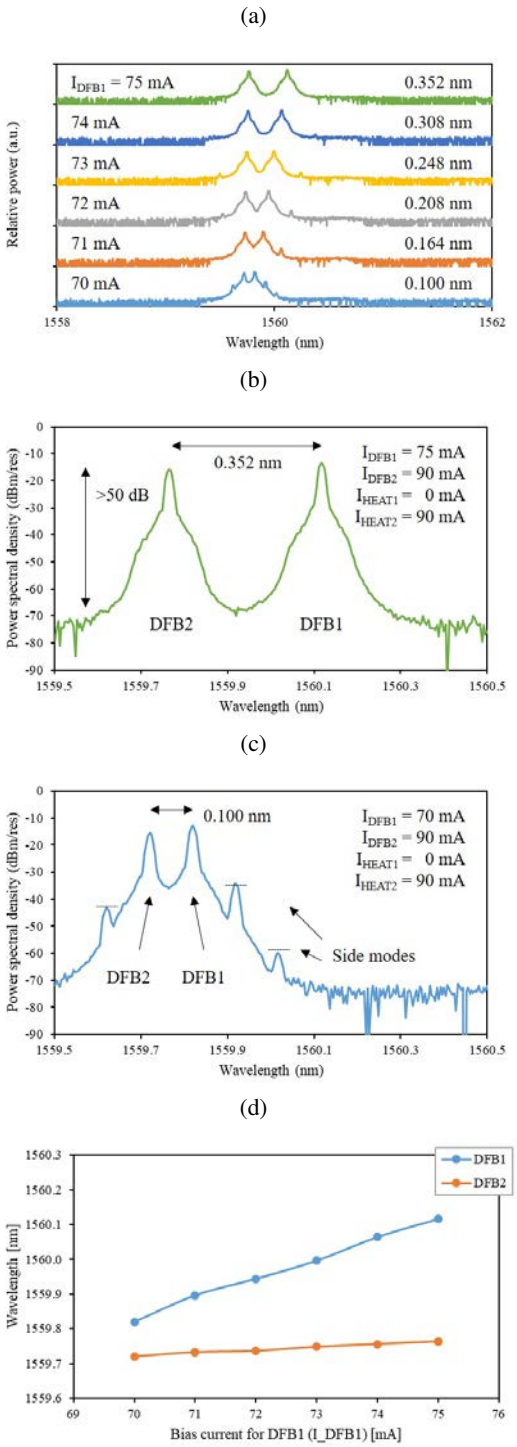

Fig. 7: Two-tone emission spectra (a) under I_{DFB1} = 75 - 70 mA. (b) under I_{DFB1} = 75 mA. (c) under I_{DFB1} = 70 mA. resolution bandwidth (res) = 0.02 nm.

with I_{DFB1} swept from 75 mA to 70 mA and the rest of bias condition is kept the same. Fig. 7(b) is a typical two-tone laser spectrum near 1560 nm. In both DFB modes, sharp 10-dB peaks stand on top of 0.2-nm-wide 40-dB-high bases. This bell shape exhibiting the dynamic range and the resolution bandwidth is an indication of the filter factor in relation to the

diffraction grating-based monochromator used in OSA. The wavelength spacing is 0.352 nm and the suppression ratio is >50 dB. In contrast, Fig. 7(c) shows a lower spacing, 0.100 nm when a lower I_{DFB1} is used. Besides, it should be noted that a few side modes have been observed. The side modes appear related to nonlinear effects. These four wave mixing (FWM)-like side modes should be caused by cross-injection between the two laser, and the cross-injection could be associated with parasitic back-reflections at coupling interfaces such as cleaved facet, butt-joints, MMI coupler , and PIN-PD. Building blocks with reduced parasitic back-reflections are preferable in this case [20]. The side modes - intermodulation products take place adjacent to the two optical tones at $2f_1$ - f_2 and $2f_2$ - f_1 where f_1 is the frequency of DFB1 and f_2 is the frequency of DFB2. The evolution of side modes can be seen in Fig. 7(a). The side modes disappear as I_{DFB1} is over 74 mA, where the frequency offset between two laser modes is already larger than the modulation bandwidth of laser. Fig. 7(d) exhibits the emission wavelengths of DFB1 and DFB2. DFB1 wavelength shifts upwards by 0.0582 nm/mA as I_{DFB1} increases. However, DFB2 also slightly moves upwards (0.0087 nm/mA) due to thermal crosstalk, as the two DFB BBs are separated by only <0.5 mm on the same substrate. Under such bias conditions the beat-note frequency covers 12 - 43 GHz (0.100 - 0.352 nm) following a nearly linear trend with respect to I_{DFB1}.

For evaluation of stability, the linewidths of both DFBs are quantified with the self-heterodyne measurement method as shown in Fig. 8(a). The light out of the PIC collected with the lensed fiber is first passed through an erbium-doped fiber amplifier (EDFA) followed by a 3-dB optical coupler. Then, in the asymmetric Mach-Zehnder interferometer (MZI) structure formed with the pair of 3-dB optical couplers, the acousto-optic modulator (AOM) is modulated at 5 GHz, and an 8-km single-mode fiber as optical delay line is used to break the coherence state. The polarization controller (PC) matches the polarization state of light coming from the two arms of MZI, optimizing the signal intensity at the photodetector (PD) prior to the radio frequency amplifier (RFA). The 5-GHz beat note is measured on the electrical spectrum analyzer (ESA), from which the optical linewidth is estimated based on that the optical linewidth is half the electrical beat note linewidth.

Under I_{DFB1} = 100 mA and I_{HEAT1} = 80 mA, the self-heterodyne RF beat note of DFB1 is shown in Fig. 8(b). The electrical FWHM (Full Width at Half Maximum) linewidth is around 70 MHz, assuming a Gaussian line shape. The electrical FWHM linewidths of DFB1 and DFB2 under various bias conditions are plotted in Fig. 8(c) and Fig. 8(d), respectively. In general, the electrical FWHM linewidth is lower than 80 MHz and increases as gain bias current or heater bias current increases. The self-heterodyne measurements demonstrate that the optical linewidth of DFB laser in the presented technology is estimated to be around $20 \sim 40$ MHz, based on the fact that the self-heterodyne electrical linewidth is approximately two times the optical linewidth. The measured linewidth appears reasonably wider compared to previous works in the same technology [13] ($\sim$10 MHz) and in the private III-V lab dedicated fabrication technology [21] ($\sim$1 MHz). With an ultra low noise current source to drive the laser, the linewidth is potentially improvable.

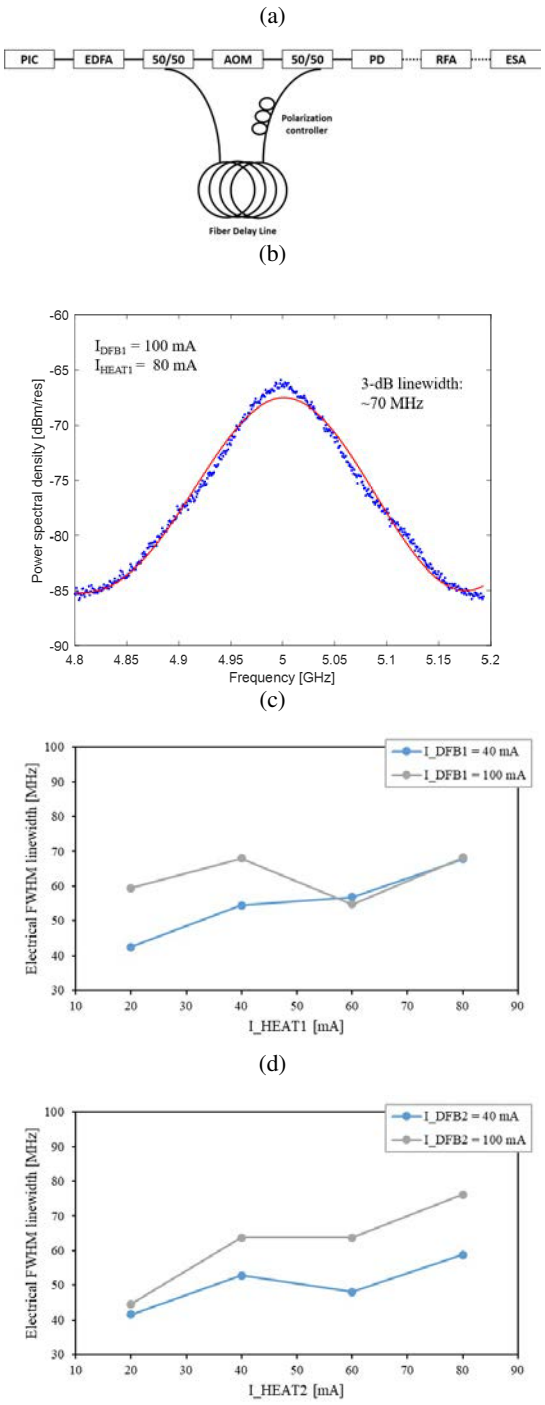

Fig. 8: (a) Laser linewidth measurement setup: delayed self-heterodyne Mach-Zehnder interferometer. (b) Self-heterodyne spectrum at 5 GHz on ESA. (c) Self-heterodyne linewidth of DFB1. (d) Self-heterodyne linewidth of DFB2.

Testing of the on-chip microwave generation via O/E conversion is carried out with a MPI ground-signal-ground (GSG) probe for the PIN-diode. The GSG probe is then connected to the RF port of an Anritsu bias tee. Through the DC port of bias tee, the PIN-diode is reverse-biased with a Keithley programmable DC source at -5.0 V. The DC + RF signal is

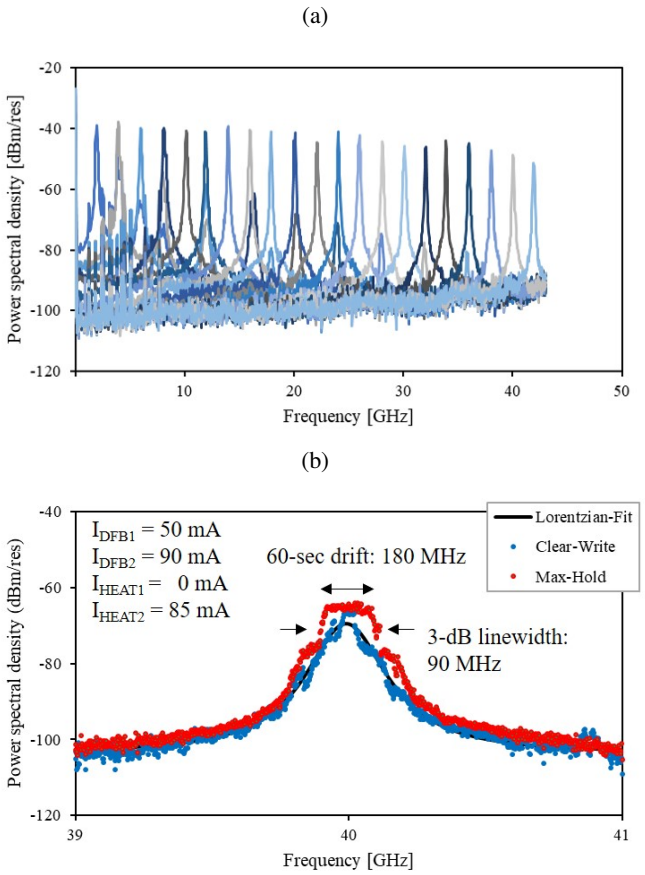

Fig. 9: (a) Continuously tunable RF beat note from 2 to 42 GHz. RBW = 100 kHz. VBW = 30 kHz. (b) RF beat note at 40 GHz. RBW = 1 kHz. VBW = 1 kHz

seen at the combined port, and sent to a Rhode and Schwarz Spectrum Analyzer (ESA) for measurement. Fig. 9(a) depicts the continuously tunable RF tone with a suppression of >50 dB ranging from 2 to 42 GHz, limited by the bandwidth of ESA. The frequency tuning is realized through properly biasing DFB1 and DFB2 as described above. Fig. 9(b) shows the beat note at 40 GHz, under I_{DFB1} = 50 mA, I_{HEAT1} = 0 mA, I_{DFB2} = 90 mA, and I_{HEAT2} = 85 mA. The Lorentzian curve fitted well with the experimental result exhibits a 3-dB linewidth of 90 MHz, related to fluctuations of the RF phase. And the max-hold trace recorded within one minute presents a flat plateau of 180 MHz, representing the frequency instability possibly due to temperature drift. It suggests that an stabilization scheme is desirable to lock the RF tone.

IV. Conclusion

A monolithically integrated III-V PIC composed of tunable lasers and high-speed photodiode has been demonstrated to obtain continuously tunable RF generation. The coupling efficiency can be further improved by replacing the lensed fiber with a cleaved standard single-mode fiber. By use of the generic foundry approach, the wavelength tuning range of >4 nm in each DFB laser and the initial set wavelength offset of ∼4 nm allow for a wavelength spacing range up to 10.7 nm. Thermal crosstalk is observed to neutralize the tuning efficiency, and nonlinearity leads to unforeseen side modes. Both lasers exhibit self-heterodyne linewidths below 80 MHz. Such a device supports on-chip O/E conversion with the PIN diode providing microwave generation that cannot be perceived beyond the bandwidth of ESA, ∼42 GHz. The generated beat note exhibits a relatively wide 90-MHz RF linewidth and 180-MHz frequency drift which are yet to be improved. For most applications in which a stable absolute frequency is desirable, the two free-running lasers must be mutually correlated to reduce the phase noise and construct the spectral coherence. Future improvements should be performed for stabilizing the free-running lasers, such as phase-locked loops (PLL) [22][23], and optical injection locking (OIL) [24][25]. Also, spectral stabilization of two integrated InP/Polymer single wavelength lasers has recently been demonstrated through OIL to a bulky optical frequency comb (OFC), in which the THz FWHM linewidth was successfully reduced from MHz to kHz [26] and the concept has long been developed [27]. It is worth highlighting that monolithically integrated mode-locked lasers (MLLs) producing OFCs have been reported in the same InP generic foundry approach [28],suggesting the device presented in this paper has the development potential to be combined with such an InP MLL-based OFC generator for greater stability without sacrificing the tunability .

Acknowledgment

This project has received funding from the European Union's Horizon 2020 research and innovation programme under the Marie Skłodowska-Curie grant agreement No. 642355 FiWiN5G. We thank Frédéric van Dijk, David de Felipe, Francisco Soares, Daan Lenstra, Sebastián Rodríguez, Shi Jia, Deming Kong, and Hao Hu for helpful discussions.

References

[1] J. Capmany and D. Novak, "Microwave photonics combines two worlds," *Nature photonics*, vol. 1, no. 6, p. 319, 2007.
[2] J. Yao, "Microwave photonics," *Journal of Lightwave Technology*, vol. 27, no. 3, pp. 314–335, 2009.
[3] T. S. Rappaport, S. Sun, R. Mayzus, H. Zhao, Y. Azar, K. Wang, G. N. Wong, J. K. Schulz, M. Samimi, and F. Gutierrez, "Millimeter wave mobile communications for 5g cellular: It will work!" *IEEE access*, vol. 1, pp. 335–349, 2013.
[4] J. G. Andrews, S. Buzzi, W. Choi, S. V. Hanly, A. Lozano, A. C. Soong, and J. C. Zhang, "What will 5g be?" *IEEE Journal on selected areas in communications*, vol. 32, no. 6, pp. 1065–1082, 2014.
[5] A. J. Seeds and K. J. Williams, "Microwave photonics," *Journal of Lightwave Technology*, vol. 24, no. 12, pp. 4628–4641, 2006.
[6] T. Nagatsuma and G. Carpintero, "Recent progress and future prospect of photonics-enabled terahertz communications research," *IEICE Transactions on Electronics*, vol. E98.C, no. 12, pp. 1060–1070, 2015.
[7] T. Nagatsuma, G. Ducournau, and C. C. Renaud, "Advances in terahertz communications accelerated by photonics," *Nature Photonics*, vol. 10, no. 6, p. 371, 2016.
[8] D. Marpaung, C. Roeloffzen, R. Heideman, A. Leinse, S. Sales, and J. Capmany, "Integrated microwave photonics," *Laser & Photonics Reviews*, vol. 7, no. 4, pp. 506–538, 2013.
[9] G. Carpintero, R. C. Guzmán, C. Gordón, G. Kervella, M. Chitoui, and F. V. Dijk, "Photonic integrated circuits for radio-frequency signal generation," *Journal of Lightwave Technology*, vol. 34, no. 2, pp. 508–515, Jan 2016.
[10] T. Nagatsuma and G. Carpintero, "Recent progress and future prospect of photonics-enabled terahertz communications research," *IEICE Transactions on Electronics*, vol. 98, no. 12, pp. 1060–1070, 2015.

[11] M. Theurer, T. Göbel, D. Stanze, U. Troppenz, F. Soares, N. Grote, and M. Schell, "Photonic-integrated circuit for continuous-wave thz generation," *Opt. Lett.*, vol. 38, no. 19, pp. 3724–3726, Oct 2013.
[12] F. van Dijk, G. Kervella, M. Lamponi, M. Chtioui, F. Lelarge, E. Vinet, Y. Robert, M. J. Fice, C. C. Renaud, A. Jimenez, and G. Carpintero, "Integrated inp heterodyne millimeter wave transmitter," *IEEE Photonics Technology Letters*, vol. 26, no. 10, pp. 965–968, May 2014.
[13] M. Sun, S. Tan, F. Guo, S. Liu, Q. Kan, D. Lu, R. Zhang, W. Zhao, S. Liang, W. Wang, R. Broeke, F. M. Soares, and C. Ji, "Integrated four-wavelength dfb diode laser array for continuous-wave thz generation," *IEEE Photonics Journal*, vol. 8, no. 4, pp. 1–8, Aug 2016.
[14] G. Carpintero, S. Hisatake, D. d. Felipe, R. Guzman, T. Nagatsuma, N. Keil, and T. Göbel, "Photonics-based millimeter and terahertz wave generation using a hybrid integrated dual dbr polymer laser," in *2016 IEEE MTT-S International Microwave Symposium (IMS)*, May 2016, pp. 1–3.
[15] J. Hulme, M. Kennedy, R.-L. Chao, L. Liang, T. Komljenovic, J.-W. Shi, B. Szafraniec, D. Baney, and J. E. Bowers, "Fully integrated microwave frequency synthesizer on heterogeneous silicon-iii/v," *Opt. Express*, vol. 25, no. 3, pp. 2422–2431, Feb 2017.
[16] J. Xu, L. Hou, Q. Deng, L. Han, S. Liang, J. H. Marsh, and H. Zhu, "Fully integrated multi-optoelectronic synthesizer for thz pumping source in wireless communications with rich backup redundancy and wide tuning range," *Scientific reports*, vol. 6, p. 29084, 2016.
[17] M. Smit, X. Leijtens, H. Ambrosius, E. Bente, J. Van der Tol, B. Smalbrugge, T. De Vries, E.-J. Geluk, J. Bolk, R. Van Veldhoven *et al.*, "An introduction to inp-based generic integration technology," *Semiconductor Science and Technology*, vol. 29, no. 8, p. 083001, 2014.
[18] N. Grote, M. Baier, and F. Soares, "Photonic integrated circuits on inp," in *Fibre Optic Communication*. Springer, 2017, pp. 799–840.
[19] A. Kumar and S. Aditya, "Performance of s-bends for integrated-optic waveguides," *Microwave and Optical Technology Letters*, vol. 19, no. 4, pp. 289–292, 1998.
[20] E. Kleijn, D. Melati, A. Melloni, T. de Vries, M. K. Smit, and X. J. Leijtens, "Multimode interference couplers with reduced parasitic reflections," *IEEE Photonics Technology Letters*, vol. 26, no. 4, pp. 408–410, 2014.
[21] F. van Dijk, A. Accard, A. Enard, O. Drisse, D. Make, and F. Lelarge, "Monolithic dual wavelength dfb lasers for narrow linewidth heterodyne beat-note generation," in *Microwave Photonics, 2011 International Topical Meeting on & Microwave Photonics Conference, 2011 Asia-Pacific, MWP/APMP*. IEEE, 2011, pp. 73–76.
[22] K. Balakier, L. Ponnampalam, M. J. Fice, C. C. Renaud, and A. J. Seeds, "Integrated semiconductor laser optical phase lock loops," *IEEE Journal of Selected Topics in Quantum Electronics*, vol. 24, no. 1, pp. 1–12, 2018.
[23] S. Arafin and L. A. Coldren, "Advanced inp photonic integrated circuits for communication and sensing," *IEEE Journal of Selected Topics in Quantum Electronics*, vol. 24, no. 1, pp. 1–12, 2018.
[24] G. Kervella, F. Van Dijk, G. Pillet, M. Lamponi, M. Chtioui, L. Morvan, and M. Alouini, "Optoelectronic cross-injection locking of a dual-wavelength photonic integrated circuit for low-phase-noise millimeter-wave generation," *Optics letters*, vol. 40, no. 15, pp. 3655–3658, 2015.
[25] A. Thorette, P. Primiani, M. Romanelli, M. Alouini, F. Van Dijk, and M. Vallet, "Self-stabilized optoelectronic oscillator using optical feedback on integrated heterodyne source," in *Lasers and Electro-Optics Europe & European Quantum Electronics Conference (CLEO/Europe-EQEC, 2017 Conference on)*. IEEE, 2017, pp. 1–1.
[26] G. Carpintero, S. Hisatake, D. de Felipe, R. Guzman, T. Nagatsuma, and N. Keil, "Wireless data transmission at terahertz carrier waves generated from a hybrid inp-polymer dual tunable dbr laser photonic integrated circuit," *Scientific reports*, vol. 8, no. 1, p. 3018, 2018.
[27] S. Fukushima, C. Silva, Y. Muramoto, and A. J. Seeds, "Optoelectronic millimeter-wave synthesis using an optical frequency comb generator, optically injection locked lasers, and a unitraveling-carrier photodiode," *Journal of lightwave technology*, vol. 21, no. 12, pp. 3043–3051, 2003.
[28] M.-C. Lo, R. C. G. Martínez, and G. Carpintero, "Monolithic mode locked laser-based optical frequency comb for ofdm integrated on inp generic technology platform," in *Optical Fiber Communication Conference*. Optical Society of America, 2018, pp. Th1I–1.